Searching for the $T^{-3/2}$ Suprathermal Power Law Tail in Parker Solar Probe's IS⊙IS Data

A. Merrill

May 20, 2020

Abstract

Results from the Advanced Composition Explorer (ACE) and the Ulysses spacecraft suggested the existence of a pervasive power-law spectrum of suprathermal ions in the solar wind with a spectral index of $-\frac{3}{2}$. This distribution is of particular interest to humanity because the suprathermal ions it describes can serve as the seed population for large, destructive events that can harm ground- and air-based equipment. It has been suggested that various statistical mechanisms can produce the observed spectrum, however the underlying physical phenomena are not yet known. The spectrum of suprathermal ions is relatively unstudied closer to the Sun than 1 au. I investigate the first year and a half of Parker Solar Probe's data to find evidence of this spectrum in this previously unstudied region. I find weak evidence to suggest the existence of a common spectrum of protons from 60 to 200 keV inside the region being studied. Naive fits to all of the events fail to produce the expected $-\frac{3}{2}$, yet some relationship between magnetic turbulence and spectral index is found, as is an apparent relationship between radial distance and spectral index, suggesting some type of asymptotic approach to index $-\frac{3}{2}$ as radial distance increases. Additionally, my results are not incompatible with recent adaptations to some statistical models that yield softer spectra. Further work is required to uncover the phenomena in this region that determine the shape of the solar wind spectrum.

1 Introduction

The solar wind in regions above 0.3 au has been studied directly [*McComas et al.*, 2007], and a considerable understanding of the population of solar wind particles and their distributions has

been gained about these regions [*Giacalone et al.*, 2002; *McComas et al.*, 2007]. One particular phenomenon that our current understanding of accelerating processes in the solar wind fails to explain is the existence of a pervasive power law spectrum of solar wind speed with a spectral index of -5; alternatively, this can be expressed as a power law of particle energy with spectral index of $-\frac{3}{2}$ [*Fisk and Gloeckler*, 2012].

1.1 The Seed Population and its Significance

Observations from ACE show significant differences in the composition of solar energetic particle (SEP) events and solar wind [*Mewaldt et al.*, 2012]. Additionally, SEPs have been measured to have densities of ^{3}He and He^+ much greater than thermal solar wind (ie. ^{3}He is an ion abundant in flares with energy $>10\,\mathrm{keV}$ and He^+ is an interstellar pickup ion), and thus loan themselves to be used as tracers of the source material of the SEP. Finally, the heavy ion composition of SEP events correlates significantly with background suprathermal densities. These results suggest that SEPs draw their source material from the suprathermal region [*Desai et al.*, 2006]. The population of ions in the suprathermal region responsible for the acceleration of SEP events has been coined the *seed population*.

The seed population, having the potential to create large SEP events, is of particular interest to human affairs as these large events can cause significant material and economic damage. For example, global satellite infrastructure, the electric power grid, and radio communications can be disrupted or destroyed by the effects of large SEP events [*National Research Council et al.*, 2013; *Desai and Giacalone*, 2016]. During major magnetic storms induced by large SEP events, atmospheric chemistry at and around the poles can be changed such that significant enhancements in the production and concentration of nitrogen dioxide is observed [*National Research Council et al.*, 2013]. Nitrogen dioxide plays an important role in the equilibrium of ozone maintained in the upper atmosphere, the maintenance of which is crucial in protecting the health of humans on the ground as well as crops and food sources. Additionally, large SEP events can expose astronauts to many times the safe limits for radiation exposure [*National Research Council et al.*, 2013], creating a problem needing to be addressed before the advent of truly accessible, commercial spaceflight. Because of the dangerous potential of SEP events, it is a goal of the Committee on a Decadal

Strategy for Solar and Space Physics to build an understanding of the creation of these large SEP events so they can be predicted, allowing us to better protect the assets of society.

1.2 The Quiet Time Spectrum

Fisk and Gloeckler [2008] propose a model acceleration of the solar wind during quiet times in which particles are accelerated in compressional turbulence which exhibits the observed spectral index of $-\frac{3}{2}$. Quiet times are defined to exclude times of increased particle flux due to acceleration from shocks or large-scale compression regions, while still maintaining sufficient fluxes to observe a spectrum. In particular, *Fisk and Gloeckler* [2008] use the following model for quiet time events:

$$j = j_0 T^{-\frac{3}{2}} \exp(-T/T_0), \tag{1}$$

where j_0 is a normalization constant, T is the energy per nucleon, and T_0 is defined as

$$T_0 = \frac{\left\langle \partial u^2 \right\rangle}{r_{g0}} \frac{Q}{A} \frac{r_0}{u_{sw}} \frac{m_p v_0}{2}, \tag{2}$$

where r_{g0} is the gyroradius of a proton evaluated at speed v_0 and location r_0, A is the mass number and Q is the charge number, and m_p is the proton mass.

Schwadron et al. [2010] demonstrate how the spectral index $-\frac{3}{2}$ could also arise from various different phenomena from those cited in *Fisk and Gloeckler* [2008]. *Schwadron et al.* [2010] demonstrate how the superposition of exponential and Gaussian distributions can show power law tails, and subsequently how various phenomena contribute to this. In particular, *Schwadron et al.* [2010] show how the same spectral shape can arise from a series Poisson-like processes in which entropy is maximized, a series of Gaussian distributions in which entropy is maximized, or a series of diffusively accelerated particle spectra with individual spectra derived from being subjected to numerous shocks. *Schwadron* [2019] elaborates how the superposition of the various processes described in *Schwadron et al.* [2010] can also result in softer spectra than the pervasive $-\frac{3}{2}$.

1.3 Instrumentation

Parker Solar Probe (PSP) provides a previously unseen view of the solar wind inside Earth's orbit. Diving from more than 60 to less than 10 $R_\odot$, the spacecraft plunges into the solar corona to observe the phenomena that accelerate the solar wind and inflate the heliosphere. PSP's closer view of the Sun can help explain how the corona is heated and how this power law spectrum is created in the solar wind [*McComas et al.*, 2014, 2007].

ACE and Ulysses have performed extensive surveys of the regions at 1 au and between 1 and ~6 au, respectively, that are thus far satisfactory for scientific goals [*McComas et al.*, 2007]. However, Prior to PSP, our closest equatorial observations of the Sun were performed by the Helios spacecrafts beginning in the late 1970s [*McComas et al.*, 2007]. Since the launch of the pair of observing spacecraft, particle detector technology has continued to progress. PSP is equipped with detectors with dramatically increased time and energy resolution, as well as being capable of discerning particle species from the solar wind [*McComas et al.*, 2014].

I use data from PSP's IS⊙IS EPI-Lo instrument to look for the existence of the common power law tail inside 1 au. EPI-Lo is a time-of-flight based mass-spectrometer capable of measuring ions and electrons varying from approximately 20 keV to 5 MeV. Of interest here are EPI-Lo's specific capabilities surrounding protons, for which the instrument is capable of measuring between 0.04 and 7 MeV [*McComas et al.*, 2014]. EPI-Lo is made of eight 45° wedge segments, each of which has 10 entrances for particles to strike a solid state detector. I use EPI-Lo's Channel T data, which is a time-of-flight (ie. SSD not used) total ion channel calibrated assuming only hydrogen.

2 Analysis

At the time of beginning the analysis, data from the beginning of PSP's flight (end of September 2019) through early January 2020 were available. Events were selected by plotting a spectrogram of hourly- and directionally-averaged time-of-flight high energy resolution proton fluxes (Channel T Flux in the IS⊙IS EPI-Lo Level 2 dataproducts) against time and energy for the entire duration of time for which data was available. Fifteen events were found in PSP's data during this time, the parameters for which can be found in Table 1. The spectrogram from which events were selected

is shown in Figure 1. Increased flux is apparent on a periodic basis occurring approximately every 5 months. This coincides with solar encounters and has little relation to actual events.

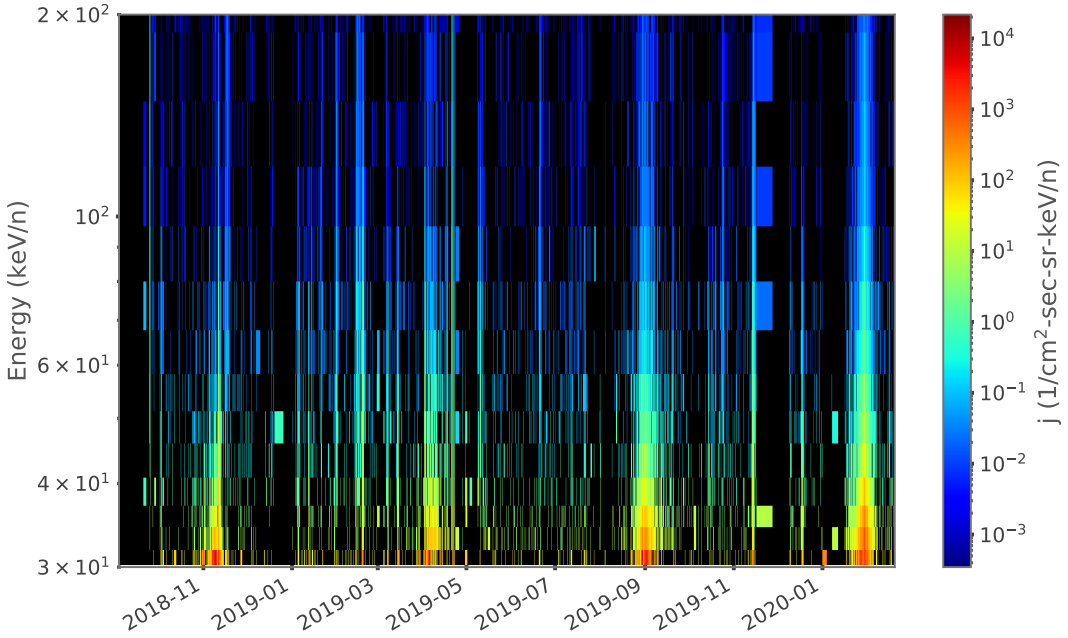

Figure 1: Flux (j) versus energy and time for the duration of the mission at the time data analysis was started. Individual events generally lasted for the approximate duration of a few days, making them too small to indicate on the spectrogram. Notice that solar encounters are visible occurring approximately every 5 months starting in November 2018.

Fisk and Gloeckler [2008] suggest a model of compressional acceleration in solar wind turbulence that predicts a functional dependence of flux on energy in the suprathermal tail as shown in Equation 1. Here, I fit the event spectra to

$$j = \tilde{j_0} T^{\alpha}, \tag{3}$$

where $\tilde{j_0}$ is a normalization constant and α is the spectral index, and both $\tilde{j_0}$ and α are fit parameters. This simplifies the analysis without loss of validity as parameters included in Equation 1 are included in $\tilde{j_0}$.

Event	Start	Stop	Spec. Index	R (au)	Peak Flux (n/keV cm^2 s sr)	η^2
0	2018-09-25 01:54	2018-09-25 22:57	-2.06	0.81	$5.49 \cdot 10^1$	$3.27 \cdot 10^{-2}$
1	2018-11-11 01:39	2018-11-12 01:36	-5.99	0.24	$1.36 \cdot 10^3$	$3.45 \cdot 10^{-2}$
2	2018-11-15 16:33	2018-11-19 23:37	-2.08	0.38	$5.68 \cdot 10^1$	$1.61 \cdot 10^{-2}$
3	2019-01-31 00:21	2019-02-01 17:00	-3.70	0.92	$5.97 \cdot 10^1$	n/a
4	2019-02-13 17:43	2019-02-18 00:03	-3.12	0.85	$6.05 \cdot 10^1$	n/a
5	2019-02-18 05:00	2019-02-19 20:55	-5.06	0.83	$2.16 \cdot 10^2$	n/a
6	2019-03-06 09:17	2019-03-08 05:04	-5.82	0.67	$6.89 \cdot 10^1$	$2.49 \cdot 10^{-2}$
7	2019-03-13 23:33	2019-03-15 12:34	-6.29	0.56	$1.07 \cdot 10^2$	$1.07 \cdot 10^{-1}$
8	2019-04-02 05:44	2019-04-03 00:36	-8.34	0.18	$4.00 \cdot 10^3$	$1.30 \cdot 10^{-2}$
9	2019-04-04 02:36	2019-04-04 20:01	-5.46	0.17	$7.45 \cdot 10^2$	$4.21 \cdot 10^{-3}$
10	2019-04-17 15:36	2019-04-18 06:51	-5.21	0.41	$1.20 \cdot 10^2$	n/a
11	2019-04-20 10:58	2019-04-23 19:32	-3.21	0.49	$7.14 \cdot 10^1$	$1.12 \cdot 10^{-2}$
12	2019-06-19 15:10	2019-06-21 22:20	-3.03	0.94	$4.53 \cdot 10^1$	n/a
13	2019-10-22 11:09	2019-10-26 08:04	-2.62	0.88	$4.51 \cdot 10^1$	n/a
14	2019-11-13 08:30	2019-11-16 22:08	-4.88	0.94	$1.04 \cdot 10^2$	n/a

Table 1: Parameters of the fifteen events identified. Events for which magnetic field data was unavailable show n/a for η^2. Peak flux was determined from the maximum across the entire energy range of EPI-Lo of the average over time and look direction.

2.1 Duration and Directionally Averaged Fits

The first approach to find evidence of the model in Equation 3 fitting the spectra of the events was to simply apply a fit to the data between 40 and 160 keV of an event-duration- and directionally-averaged spectrum of each event. This energy region was determined by visual inspection of the events to to fit the region most like a power-law inside the suprathermal region described by *Fisk and Gloeckler* [2008]. This yielded fits like those shown in Figure 2. The exponents of these fits did not match well to the expected $-\frac{3}{2}$.

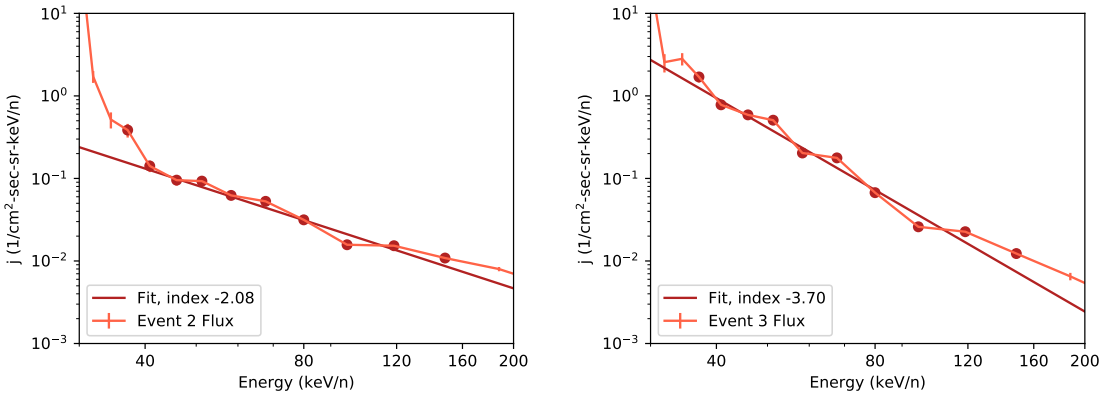

(a) Event 2 (b) Event 3

Figure 2: Fits of the spectra from Events 2 and 3. Red points on the spectrum of either plot indicate points used for the fit.

2.2 Magnitude and Direction of B

Fisk and Gloeckler [2008] note that the common spectrum appears in populations of charged particles subject to non-shock (ie. quiet time) acceleration. Accordingly, it became necessary distinguish shock and large compressional events from quiet time events. Analysis by *Cohen et al.* [2020] and other suggest that the Event 1, shown in Figure 3, is the result of a CIR. Work towards identifying the histories of each event in order to classify quiet time from non-quiet time events is in progress.

2.3 η^2 and Magnetic Turbulence

I considered magnetic variance acting as a proxy for magnetic turbulence to indicate accelerating processes in the region of the spacecraft. *Schwadron et al.* [1996] suggest the statistical quantity

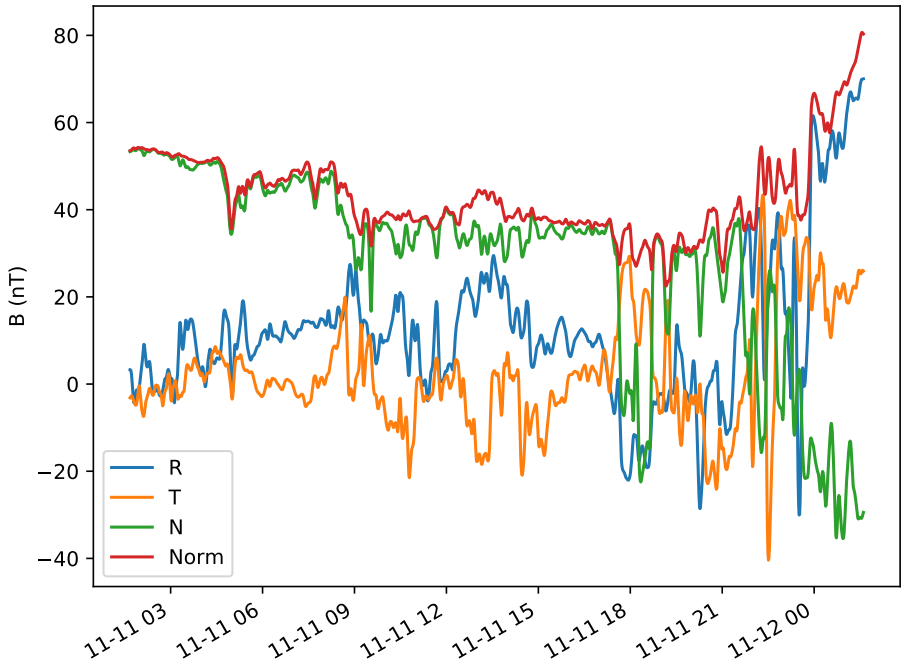

Figure 3: Event 1. Analysis by *Cohen et al.* [2020] and others suggest this is a CIR.

η^2 to act as a proxy of magnetic turbulence. Magnetic turbulence indicates the relative strength of acceleration associated with the phenomenon [*Fisk and Gloeckler*, 2006]. Plots of B can be found in Figure 3, and plots of η^2 are shown in Figure 4. An association between magnetic variance and spectrum harness was not found. However, an apparent upper limit as a function of radius seems to be present in Figure 4b.

2.4 Spectral Index versus Radius

I finally considered a relationship between radius and spectral index. A plot of this data can be seen in Figure 5. An apparent "spectral hardening" occurs as radius increases: events appear to have less negative power laws when their flows are observed at greater radii. Furthermore, this seems to be consistent with the relationship between turbulence and radius observed in Figure 4. This would suggest that as mechanics in the solar wind drive greater and greater turbulence at larger radii, the spectrum hardens as ions accelerate.

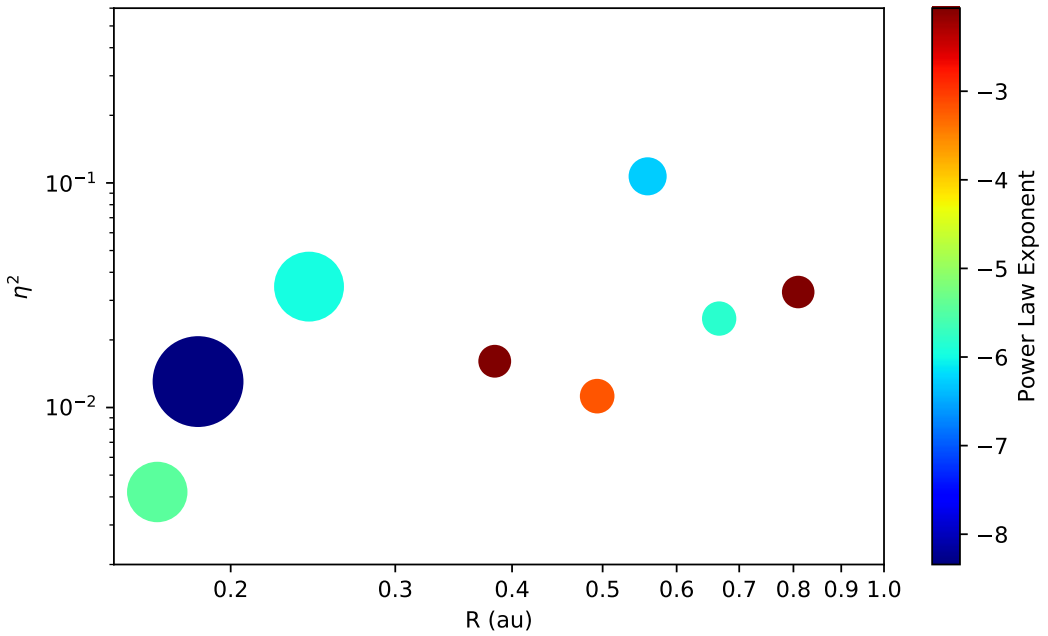

(a) Variance of magnetic field versus radial distance for each event compared with its peak flux and its spectral index. Size indicates peak flux, color indicates spectrum hardness. *Schwadron et al.* [1996] propose magnetic variance η^2 to be a proxy for plasma turbulence. It appears that a trend exists such that events closer to the sun have less variance in the magnetic field. Events for which magnetic field data was not available are not shown.

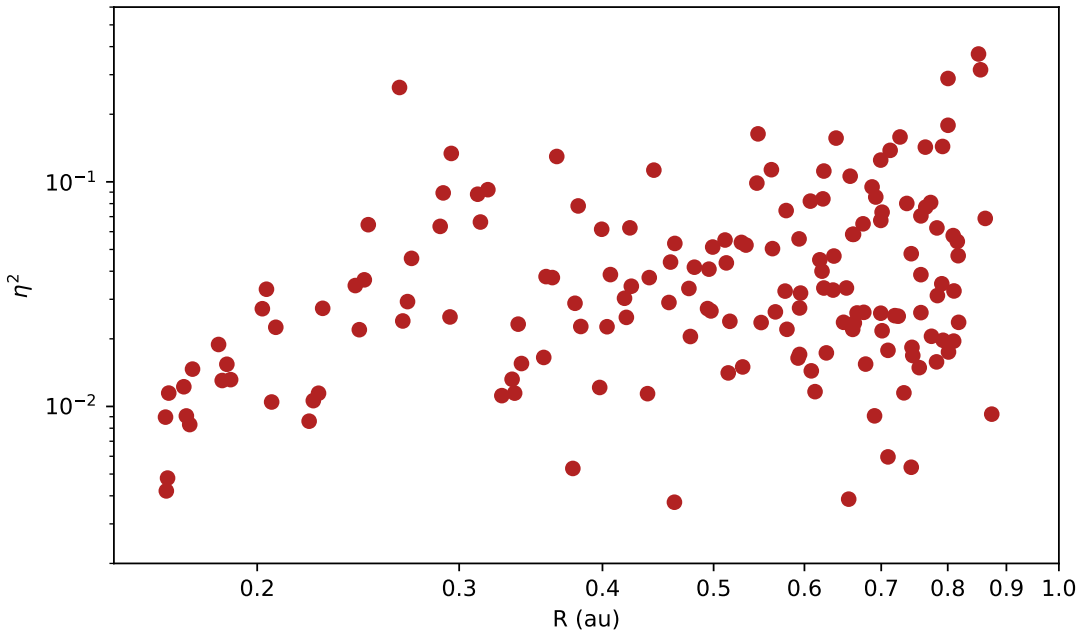

(b) Variance of magnetic field versus radial distance for each day included in the analysis, (ie. mid September 2018 to January 2020). The apparent upper limit of magnetic turbulence as a function of radius seen in Figure 4a is even more apparent here.

Figure 4: η^2 versus radial distance.

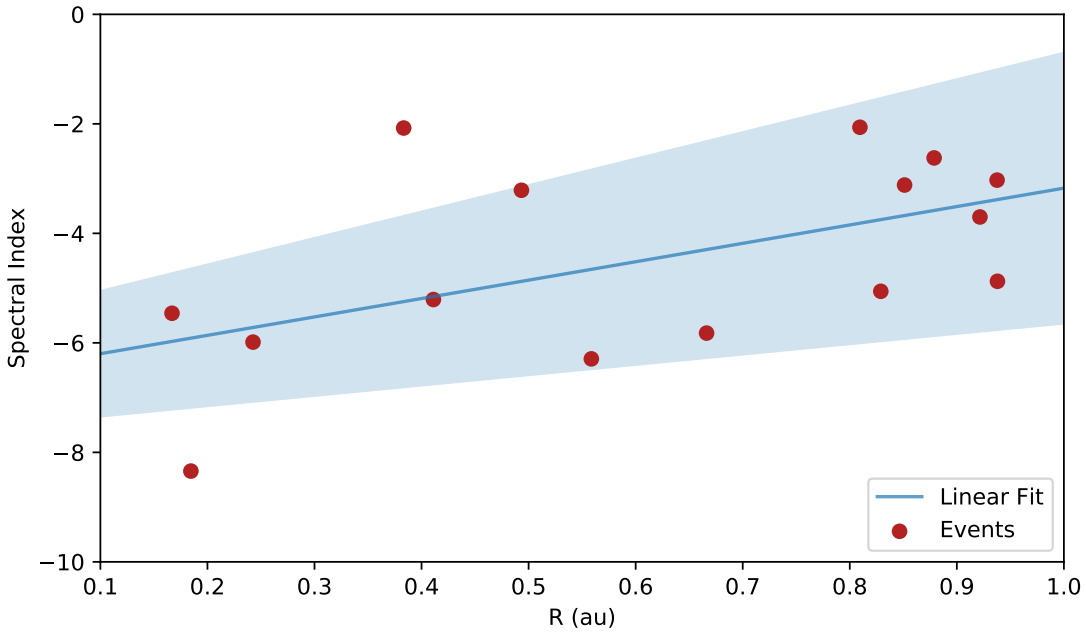

Figure 5: An apparent relation between radial distance R and the spectral index can be seen in the event data. Locally this relationship can be modeled by a line, though this is demonstrably not the case at greater radii as the spectral index approaches $-\frac{3}{2}$ [*Fisk and Gloeckler*, 2008, 2006; *Schwadron et al.*, 2010; *Schwadron*, 2019]. This fit suggests that spectral index $-\frac{3}{2}$ may be approached by an asymptote with respect to radius. The linear fit between radius and spectral index has slope $3.0 \pm 1.5\,\mathrm{au}^{-1}$ and intercept -7.0 ± 1.0; $r^2 = 0.29$.

3 Discussion & Conclusion

I analyze proton flux data from Parker Solar Probe's first year and a half to find evidence for the common power law tail described in *Fisk and Gloeckler* [2006]. I do not find evidence to suggest a common spectrum among these data.

None of the fifteen events described in Table 1 have a spectral index near $-\frac{3}{2}$. My analysis is limited in its broad application of fits and its assumption of "generally" quiet time conditions. However, despite that this is the case, with enough events or enough data eventually serendipity would have it that we see an event with the proposed power law tail of $-\frac{3}{2}$.

Schwadron [2019] demonstrates how with reasonable assumptions it may be the case the spectral index $-\frac{3}{2}$ is the upper limit on spectral hardness for suprathermal ions in the energy range being investigated. This could serve as an explanation why such a hard spectrum is not observed in the events in the analysis.

The events found here show a clear relationship between spectral hardness and radial distance, as shown in Figure 5, despite the poor quality of this fit (ie. $r^2 = 0.29$). While it cannot be the case that this relationship is linear, the relationship in the domain that is shown suggests that the spectral index of solar wind approaches some value. Even more interesting is that the hardest *and* softest spectra occur with 0.4 au, suggesting that there may be some mechanism to "homogenize" the energy distribution of particles as they flow outward. This relationship also appears to be compatible with the results shown in Figure 4: greater magnetic turbulence in the solar wind characterizes greater acceleration, increases the spectral hardness [*Fisk and Gloeckler*, 2008].

Also of note is the apparent upper limit as a function of radial distance on magnetic turbulence as quantified by η^2. This is shown in Figure 4.

Altogether, I consider here a naive approach without disregarding any event that may include processes originally excluded in *Fisk and Gloeckler* [2008]. I search for a relation of spectral index with magnetic turbulence, quantified by η^2, and radial distance. I fail to find evidence suggesting the existence of a common spectral of suprathermal ions in the region <1.0 au. However, I find significant evidence to suggest some relationship between radial distance and spectral index and radial distance and an upper limit on magnetic turbulence.

4 Future Work

Some extensions to this study could include the following:

- Analysis on a moving average of each event may show different results or evidence of the common spectrum. This would additionally benefit from being able to compare a moving average of the spectrum and its index to radius as well.
- Compare events with other authors and observatories and exclude events on this basis, such as *Cohen et al.* [2020].

5 Acknowledgments

The author wishes to sincerely thank Dr. Jonathan Niehof and Professor Nathan Schwadron for sharing their expertise and guidance throughout the research process, without which this work could not have been accomplished. In addition, the author would like to thank Dr. Dana Filoti and Professor James Ryan for their feedback during the University of New Hampshire Undergraduate Research Conference in Physics.

This work was supported by NASA Prime Contract No. 136435.

References

Cohen, C. M. S., E. R. Christian, A. C. Cummings, et al. (2020), Energetic particle increases associated with stream interaction regions. *The Astrophysical Journal Supplement Series*, *246*(2), 20, doi:10.3847/1538-4365/ab4c38.

Desai, M. and J. Giacalone (2016), Large gradual solar energetic particle events. *Living Reviews in Solar Physics*, *13*(1), doi:10.1007/s41116-016-0002-5.

Desai, M. I., G. M. Mason, J. E. Mazur, and J. R. Dwyer (2006), The seed population for energetic particles accelerated by CME-driven shocks. *Space Science Reviews*, *124*(1-4), 261–275, doi: 10.1007/s11214-006-9109-7.

Fisk, L. A. and G. Gloeckler (2006), The common spectrum for accelerated ions in the quiet-time solar wind. *The Astrophysical Journal Letters*, *640*, L79, doi:10.1086/503293.

Fisk, L. A. and G. Gloeckler (2008), Acceleration of suprathermal tails in the solar wind. *The Astrophysical Journal*, *686*(2), 1466–1473, doi:10.1086/591543.

Fisk, L. A. and G. Gloeckler (2012), Particle acceleration in the heliosphere: Implications for astrophysics. *Space Science Reviews*, *173*(1-4), 433–458, doi:10.1007/s11214-012-9899-8.

Giacalone, J., J. R. Jokipii, and J. Kota (2002), Particle acceleration in solar wind compression regions. *The Astrophysical Journal*, *573*(2), 845–850, doi:10.1086/340660.

McComas, D. J., N. Alexander, N. Angold, et al. (2014), Integrated science investigation of the sun (ISIS): Design of the energetic particle investigation. *Space Science Reviews*, *204*(1-4), 187–256, doi:10.1007/s11214-014-0059-1.

McComas, D. J., M. Velli, W. S. Lewis, et al. (2007), Understanding coronal heating and solar wind acceleration: Case for in situ near-sun measurements. *Reviews of Geophysics*, *45*(1), doi:10.1029/2006rg000195.

Mewaldt, R. A., G. M. Mason, and C. M. S. Cohen (2012), The dependence of solar energetic particle fluences on suprathermal seed-particle densities. AIP, doi:10.1063/1.4768755.

National Research Council, Committee on a Decadal Strategy for Solar and Space Physics, Space Studies Board, Aeronautics and Space Engineering Board, and Division on Engineering and Physical Sciences (2013), *Solar and Space Physics: A Science for a Technological Society*. National Academies Press, Washington, DC, ISBN 978-0-309-16428-3, doi:10.17226/13060.

Schwadron, N. A. (2019), Kappa Distributions from the Superposition of Stochastic Processes: Applications Through the Heliosphere. In *AGU Fall Meeting Abstracts*, volume 2019, SH44A–01.

Schwadron, N. A., M. A. Dayeh, M. Desai, H. Fahr, J. R. Jokipii, and M. A. Lee (2010), Superposition of stochastic processes and the resulting particle distributions. *The Astrophysical Journal*, *713*(2), 1386–1392, doi:10.1088/0004-637x/713/2/1386.

Schwadron, N. A., L. A. Fisk, and G. Gloeckler (1996), Statistical acceleration of interstellar pick-up ions in co-rotating interaction regions. *Geophysical Research Letters*, *23*(21), 2871–2874, doi:10.1029/96gl02833.